Available online at www.sciencedirect.com
SCIENCE DIRECT®
Cryogenics 43 (2003) 369–378
Cryogenics
www.elsevier.com/locate/cryogenics

Critical examination of heat capacity measurements made on a Quantum Design physical property measurement system ☆

J.C. Lashley [a,*], M.F. Hundley [a], A. Migliori [a], J.L. Sarrao [a], P.G. Pagliuso [a], T.W. Darling [a], M. Jaime [a], J.C. Cooley [a], W.L. Hults [a], L. Morales [a], D.J. Thoma [a], J.L. Smith [a], J. Boerio-Goates [b], B.F. Woodfield [b], G.R. Stewart [c], R.A. Fisher [d], N.E. Phillips [d]

[a] *Materials Science and Technology Division, Los Alamos National Laboratory, P.O. Box 1663 MST-8, MS G721, Los Alamos, NM 87545, USA*
[b] *Department of Chemistry and Biochemistry, Brigham Young University, Provo, UT 84602, USA*
[c] *Department of Physics, University of Florida, Gainesville, FL 32611-8440, USA*
[d] *Lawrence Berkeley National Laboratory, University of California, Berkeley, CA 94720, USA*

Received 15 January 2003; accepted 21 March 2003

Abstract

We examine the operation and performance of an automated heat-capacity measurement system manufactured by Quantum Design (QD). QD's physical properties measurement system (PPMS) employs a thermal-relaxation calorimeter that operates in the temperature range of 1.8–395 K. The accuracy of the PPMS specific-heat data is determined here by comparing data measured on copper and synthetic sapphire samples with standard literature values. The system exhibits an overall accuracy of better than 1% for temperatures between 100 and 300 K, while the accuracy diminishes at lower temperatures. These data confirm that the system operates within the ±5% accuracy specified by QD. Measurements on gold samples with masses of 4.5 and 88 mg indicate that accuracy of ±3% or better can be achieved below 4 K by using samples with heat capacities that are half or greater than the calorimeter addenda heat capacity. The ability of a PPMS calorimeter to accurately measure sharp features in $C_p(T)$ near phase transitions is determined by measuring the specific heat in the vicinity of the first-order antiferromagnetic transition in Sm_2IrIn_8 ($T_o = 14$ K) and the second-order hidden order (HO) transition in URu_2Si_2 ($T_N = 17$ K). While the PPMS measures $C_p(T)$ near the second-order transition accurately, it is unable to do so in the vicinity of the first-order transition. We show that the specific heat near a first-order transition can be determined from the PPMS-measured decay curves by using an alternate analytical approach. This correction is required because the latent heat liberated/absorbed at the transition results in temperature–decay curves that cannot be described by a single relaxation time constant. Lastly, we test the ability of the PPMS to measure the specific heat of $Mg^{11}B_2$, a superconductor of current interest to many research groups, that has an unusually strong field-dependent specific heat in the mixed state. At the critical temperature the discontinuity in the specific heat is nearly 15% lower than measurements made on the same sample using a semi-adiabatic calorimeter at Lawrence Berkeley National Laboratory.

PACS: 07.20.Fw; 65.40.Ba

* Corresponding author.
E-mail address: j.lash@lanl.gov (J.C. Lashley).

0011-2275/03/$ - see front matter © 2003 Elsevier Science Ltd. All rights reserved.
doi:10.1016/S0011-2275(03)00092-4

1. Introduction

Since the pioneering work of Eucken [1] and Nernst [2] in the early 20th century, adiabatic calorimetry has provided the most accurate means of obtaining specific-heat data. The high accuracy arises from the simplicity of the measurement principle. The adiabatic measurement approach comes directly from the classical definition of heat capacity,

$$C_p = \lim_{dT\to 0}\left(\frac{dQ}{dT}\right)_p \quad (1)$$

where dQ is a heat input that causes a subsequent temperature rise dT in the sample. However, the study of novel materials, many of which can be obtained only in small amounts, has benefited from small-sample calorimetric measurements. These types of measurements are usually made using the ac method developed by Handler and co-workers in 1967 [3] and Sullivan and Seidel in 1968 [4], or by a thermal-relaxation method developed by Bachmann et al. in 1972 [5]. Since 1972 a variety of calorimeters have been implemented by the condensed-matter research community based on the thermal-relaxation method [6–8]. A fully automated relaxation calorimeter is now available commercially, the physical property measurement system (PPMS) from Quantum Design (QD) [9]. The focus of this paper is to examine the operation of the PPMS calorimeter and to compare its performance to that of conventional relaxation calorimeters based on the Bachmann approach [5].

Our combined experience in making specific-heat measurements has taught us that there are many difficulties in analyzing the individual contributions from various degrees of freedom to the specific heat at low temperatures, and such measurements demand specialized instrumentation. Consequently, there is a great deal of effort that goes into controlling the details that are part of calorimetric measurements. These include thermometry, temperature-scale issues, and the creation and control of heat leaks. In a commercially available calorimeter we anticipated that a large number of these details might be hidden from the user. This fact has motivated us to do a systematic study of PPMS calorimeter performance. Therefore, we examine specific-heat measurements made with a QD PPMS calorimeter to determine the accuracy and precision that can be obtained with this instrument. We compare the results obtained on the PPMS with results obtained on a custom-built, small-sample relaxation calorimeter, and to results from the literature. Several materials with special properties were chosen for comparison with specific-heat measurements made by other techniques. Accuracy and precision limiting values are determined from specific-heat measurements on copper single crystals, polycrystalline gold, and synthetic sapphire samples. In addition, the limitations of the thermal-relaxation method in properly measuring sharp features in the specific heat are illustrated by measuring the specific heat in the vicinity of the first-order antiferromagnetic (AF) transition at $T_N = 14$ K in Sm_2IrIn_8 [10], and the second-order HO transition at $T_o = 17$ K in the heavy-fermion URu_2Si_2 [11]. We also observe the strongly field-dependent specific heat of $Mg^{11}B_2$ by examining the discontinuity in the specific heat at the critical temperature, and by measuring the field dependence of the electronic specific heat γT. We compare the results from the PPMS to measurements made on the same sample at Lawrence Berkeley National Laboratory (LBNL) [12].

2. Thermal relaxation calorimetry

Thermal-relaxation calorimetry provides a means of determining a sample's specific heat by measuring the thermal response of a sample/calorimeter assembly to a change in heating conditions. The heat-flow diagram for a standard relaxation calorimeter [5] is depicted in Fig. 1. The experimental arrangement involves a sample of unknown heat capacity C_x that is attached to a sample platform with a thermal grease (e.g., Apiezon™ N grease). The platform consists of a thin sapphire or silicon disc, which has high thermal conductivity. A thin-film heater is evaporated onto the bottom of the platform, and the platform temperature T_p is determined from a bare temperature sensor attached to it. Wires thermally link the platform to a copper heat sink held at a constant temperature T_0. These wires serve two functions by creating a thermal link between the bath and platform with a thermal conductance K_1 and by providing a means of making electrical connections to the temperature sensor and heater. With a power P applied to the platform via the thin-film heater, the coupled differential equations

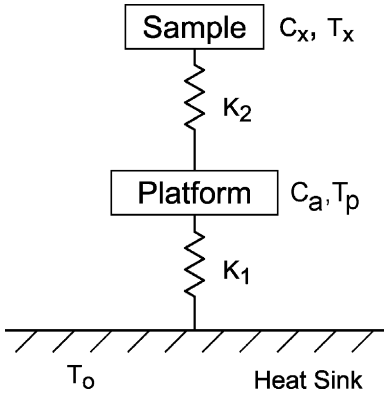

Fig. 1. Heat-flow diagram for a conventional thermal-relaxation calorimeter.

$$P = C_a \frac{dT_p}{dt} + K_2(T_p - T_x) + K_1(T_p - T_0)$$
$$0 = C_x \frac{dT_x}{dt} + K_2(T_x - T_p) \quad (2)$$

describe the heat-balance condition for the system depicted in Fig. 1. In Eq. (2), K_2 is the thermal conductance of the sample-platform thermal link, and C_a is the combined addenda heat capacity of the platform, temperature sensor, heater, and thermal-contact grease. When a power P is applied to the heater, the platform/sample assembly warms to a temperature $T_0 + \Delta T$, where $\Delta T = P/K_1$. When the thermal connection between the sample and platform is very strong ($K_2 \gg K_1$), $T_x \simeq T_p$, the heat-balance condition simplifies to

$$P = (C_a + C_x)\frac{dT_p}{dt} + K_1(T_p - T_0) \quad (3)$$

When the heat flowing to the platform is discontinued, the platform/sample assembly will cool to the bath temperature T_0 following the simple expression

$$T_p(t) = T_0 + \Delta T \exp(-t/\tau) \quad (4)$$

with a time constant $\tau = (C_x + C_a)/K_1$. As long as ΔT is small enough ($\Delta T/T \ll 1$) so that the temperature-dependence of C_x, C_a, and K_1 can be ignored, and Eq. (4) can be used to determine C_x from a measured τ. K_1 is determined by measuring the temperature change ΔT that results when power P is applied, while the addenda heat capacity C_a can be determined from a decay measurement with no sample attached to the platform. Thus, a decay cycle, consisting of the establishment of steady state at constant P and $T_p > T_0$ followed by relaxation to T_0, gives K_1 and C_x.

In practice it is often the case that the sample-platform thermal link is not sufficient to insure $K_2 \gg K_1$. In this case $T_x \neq T_p$, and the thermal decay of T_p involves the sum of two exponentials,

$$T_p(t) = T_0 + A\exp(-t/\tau_1) + B\exp(-t/\tau_2) \quad (5)$$

One of the time constants (defined as τ_2) is usually much shorter than the other. This fast process (referred to as the τ_2 effect) corresponds to thermal relaxation between the sample and the platform and the surrounding Cu ring, while the more gradual process (τ_1) arises from thermal relaxation between the platform/sample and the heat-sink temperature bath. Although the details are beyond the scope of this article, Schwall et al. [6] show that measured decay curves can be used to determine τ_1, τ_2, K_2, and C_x given known values for C_a and K_1. The process outlined above readily lends itself to computer control, which allows an extended series of decays cycles (10–100) to be averaged at each temperature to produce heat-capacity measurements that have a point-to-point scatter of less than 1%.

There are some important limitations to the approach outlined above. Because each decay cycle must extend for many time constants to ensure a steady-state initial condition and define the decay parameters, measurements can be quite time consuming if τ_1 is overly large. The Bachmann approach [5] would appear to be impractical for time constants of more than 100 s. In addition, that approach is predicated on the assumption that the sample specific heat does not vary over the temperature range encompassed by a decay cycle (i.e., $C(T) \approx C(T_0 + \Delta T)$). This will be true only when the relative change in the heat capacity over the temperature span ΔT is small, or $(\Delta T/C)(dC/dT)_{max} \ll 1$. Near a phase transition the relative change in the sample heat capacity with temperature, $(1/C_x)(dC_x/dT)_{max}$ can be large, which renders this assumption invalid. The specific heat can still be determined in the vicinity of a phase transition by analyzing the thermal-relaxation data point-by-point rather than by obtaining a single C_x value for the entire temperature region spanned by the decay. If τ_2 effects can be ignored ($K_2 \gg K_1$) (Eq. (3)) in the case where $P = 0$ and in the limit where $C_x \gg C_a$, can be rearranged to obtain

$$C_x(T) = -K_1 \frac{(T - T_0)}{dT/dt} \quad (6)$$

$C_x(T)$ can be determined near a phase transition by applying Eq. (6) to a relaxation curve regardless of how large $(1/C_x)dC_x/dT$ might be. In practice, it is useful to plot the time-dependent relaxation data $T(t)$ as $\ln[(T - T_o)/\Delta T]$ versus t. If we define the temperature-dependent slope of this plot as $\Gamma(T)$, the temperature-dependent specific heat can be calculated via Eq. (7). This approach is employed in Section 4 to analyze data near a first-order magnetic transition. We note that a similar analysis of cooling curves near first-order phase transitions has been published by Ema and co-workers for an ac/relaxation mode calorimeter [13].

$$C_x(T) = -K_1/\Gamma(T) \quad (7)$$

QD's approach to measuring specific heat is similar to that described above. The PPMS calorimeter platform consists of a thin alumina square with dimensions 3 mm × 3 mm. The platform is backed by a thin-film heater and a bare Cernox sensor™ (Lakeshore Cryotronics), while thin wires provide thermal and electrical links to the platform. The PPMS software utilizes a specified curve-fitting method [14] to determine $C_x(T)$. In this approach a single heat pulse of width $\Delta t \approx \tau_1$ is applied at $t = 0$, and the platform temperature is recorded for $0 \leqslant t \leqslant 2\tau_1$. With known values for K_1, P, and C_a, the experimental unknowns C_x and K_2 are determined analytically from the $T(t)$ data by numerically integrating the combined differential equations that characterize the system Eq. (2). The time constants τ_1 and τ_2 are calculated from C_x, C_a, K_1, and K_2 [14]. Because this calorimetric method involves taking data for

only two time constants, it can be much quicker than measurements based on the Bachmann approach, a feature that becomes significant when τ_1 is much greater than one second. As with the Bachmann approach, QD's curve-fitting technique is improved by carrying out a number of decay sweeps at each temperature and averaging the results to reduce scatter in the $C_x(T)$ data.

3. Experiment

3.1. Samples

Materials that can be obtained readily in high purity and known pedigree make a suitable choice for low-temperature, specific-heat measurement standards. We elected to use a copper single crystal and NIST gold as metallic calorimetric standards. Similarly, we used a synthetic sapphire single crystal (mass of 7.7 mg) for a non-metallic standard, which was obtained from NIST (NIST 720). The 26.3 mg copper single crystal is 99.99999% pure, and was vacuum-annealed prior to measurement. The NIST polycrystalline gold samples (SRM 685) had chemical purities of 99.999% (metals basis) with 0.0001 at% Fe. Single crystals of Sm_2IrIn_8 were chosen as a first-order transition standard both because this material has been measured previously on our custom-built relaxation calorimeter [10], and because of its sharp first-order transition at $T_N = 14.1$ K. Crystals were prepared by a flux method described elsewhere [10]. Similarly, the heavy-fermion URu_2Si_2 was chosen as a continuous (second-order) phase transition standard because it has nearly the same transition temperature $T_o = 17.5$ K [11]. Crystals of URu_2Si_2 were grown in a tri-arc furnace by the Czochralski method and annealed for eight days at 950 °C. $Mg^{11}B_2$ was used as an example of a superconductor that also has an unusually strong field-dependent specific heat in the mixed state. The powder sample of $Mg^{11}B_2$ was prepared at Argonne National Laboratory by reacting high-purity ^{11}B powder and Mg metal in a capped BN crucible at 850 °C under an argon atmosphere for 1.5 h [15].

3.2. Measurements

Specific-heat measurements were made with a PPMS using the relaxation method. In all measurements, except for the $Mg^{11}B_2$, Apiezon N grease was placed on the sample platform and weighed. C_a, including the contribution of the grease, was measured over the desired temperature range before the sample was loaded onto the platform. C_a was subtracted from the total measured heat capacity to obtain the specific heat of the sample. For $Mg^{11}B_2$, the empty platform was measured at each field. In order to obtain a thermal link with the powder, Apeizon N grease was heated and mixed with the powdered $Mg^{11}B_2$ on a microscope slide, and then transferred to the sample platform. The weights of the residual mixture of $Mg^{11}B_2$ powder and N grease not put on the platform were obtained using three hot toluene extractions. Because the grease is soluble in hot toluene and $Mg^{11}B_2$ powder is not, it could be filtered and weighed. The toluene was then evaporated leaving the residual grease for weighing. The heat capacity of the platform and the grease were subtracted from the total heat capacity. The $Mg^{11}B_2$ was magnetic field-cooled from 85 K between each set of measurements.

For the metal samples, care was taken to shape high-quality crystals to either a flat disk or a square geometry in order to obtain good thermal contact with the sample platform (i.e., $K_2 \gg K_1$). For the copper measurements, three replicate thermal-relaxation cycles were made at each temperature in order to evaluate the PPMS data reproducibility. Measurements for the phase-transition standards URu_2Si_2 and Sm_2IrIn_8 were made over a limited temperature range with thermal-relaxation decay ΔTs of approximately 0.13 K.

3.3. Thermometry

The PPMS utilizes two Lakeshore Cernox [16] temperature sensors for sample and control thermometry. Both the control and sample thermometers are used to cover the entire temperature range of the PPMS heat-capacity option ($T \approx 1.8$ to ≈ 395 K). The system control thermometer is located below the sample platform, inside the sample space. The temperature scale is based on the ITS-90 scale as replicated by Lakeshore. In general, this temperature scale gives reasonable results over a wide temperature range. However, at low temperatures we found a significant deviation from previous work originating from a thermometer-current dependence inherent in the Lakeshore scale [16]. Experience with a Cernox thermometer at LBNL has shown that rapid cooling produces irreproducible and erroneously high temperatures. For example, after rapid cooling from 50 to 8 K the thermometer read 8 mK too high, and the error decayed non-exponentially in time, more rapidly at first, but logarithmically after a few hours, reaching 4 mK after 10 h [17]. For specific-heat measurements taken in short time intervals, the error tends to cancel in ΔT and C, but care was taken to cool the thermometer slowly before making measurements to keep errors to less than a few tenths of a percent. The Cernox thermometers have a relatively weak dependence on magnetic field at temperatures of the order of 10 K and higher, but that advantage disappears at lower temperatures where the field dependence is strong [16] and not easily represented analytically.

4. Results and discussion

4.1. Calorimeter performance

Specific-heat measurements have seen many advances in the decades since the work of Eucken [1] and Nernst [2], principally in the use of high-performance measurement electronics, micro-device fabrication technology, and computer automation. However, the temperature scale continues to be the essential factor that determines accuracy and smoothness in specific-heat data. This fact arises because the fractional deviation in the specific heat caused by an error in the temperature scale is defined by the temperature derivative of this fractional error. Specifically, if T_a represents the actual temperature and T_m represents the measured temperature determined without taking into account error in the temperature scale, the fractional error in the measured specific heat $\Delta C/C$ is

$$\frac{\Delta C}{C} = -(\delta) - \frac{d\delta}{dT} T_m \tag{8}$$

where $\delta \equiv (T_m - T_a)/T_a$ is the fractional deviation in the temperature scale. While there might only be small deviations in the δ term, there can be a substantial contribution to $\Delta C/C$ from the $d\delta/dT$ term. This is particularly true below 1 K where the error in C stemming from temperature-scale error can be as high as 5%, depending on the slope in the δ versus T curve. Estimates of this error for the temperatures in the range of 4–30 K are 0.5–1%. However, above 40 K this error is quite small (less than 0.5%).

In order to compare our PPMS specific-heat results to accepted literature values, it is necessary to establish a suitable reference function that is based on the most accurate and smooth data available. The accuracy of PPMS specific-heat data is best determined by comparing values measured on a high-purity copper sample with literature values obtained using a variety of temperature scales. The basis for making comparisons is as follows: Below 30 K, the PPMS copper results were compared to the zero-magnetic field, low-temperature data of Holste et al. [18], Martin [19], and Phillips et al. [20], while above 30 K the data were compared to the high-temperature data of Martin [21]. A smooth copper reference specific-heat function containing these zero-field results, was made by averaging the data of Holste, Martin, and Phillips, and fitting the data to the expression

$$C_{ref} = \gamma T + \sum_{n=1}^{8} B_{2n+1} T^{2n+1} \tag{9}$$

from 1.8 to 30 K. Each of the low-temperature measurements used in the copper reference file was made on a temperature scale that was carefully established in the individual laboratories with an uncertainty of ±0.2%. The scatter among these three data sets is no greater than ±0.25% from 0.4 to 30 K.

A deviation plot of the low-temperature, specific-heat data for the 26.3 mg sample of vacuum-annealed, single-crystal copper obtained on the PPMS is shown in Fig. 2a. The $y = 0$ line represents the smooth copper reference function. Above 4 K, the PPMS data is generally higher than the reference data by 1.5%; below 4 K the uncertainty increases to nearly 4%. It is instructive to compare the low-temperature data by looking at the effect on the low-temperature limiting Debye temperature Θ_D and the electronic contribution, or Sommerfeld coefficient, γ. The Debye temperature is obtained from the slope of a plot of C/T versus T^2 while the y-intercept determines γ. The low-temperature PPMS Cu specific-heat data between 2 and 9.19 K are represented by a linear term $\gamma = 0.712$ mJ/mol K^2, and a T^3 term $\beta = 0.0461$ mJ/mol K^4 (corresponding to $\theta_D = 348$ K). This γ and the Debye temperature differ from those of

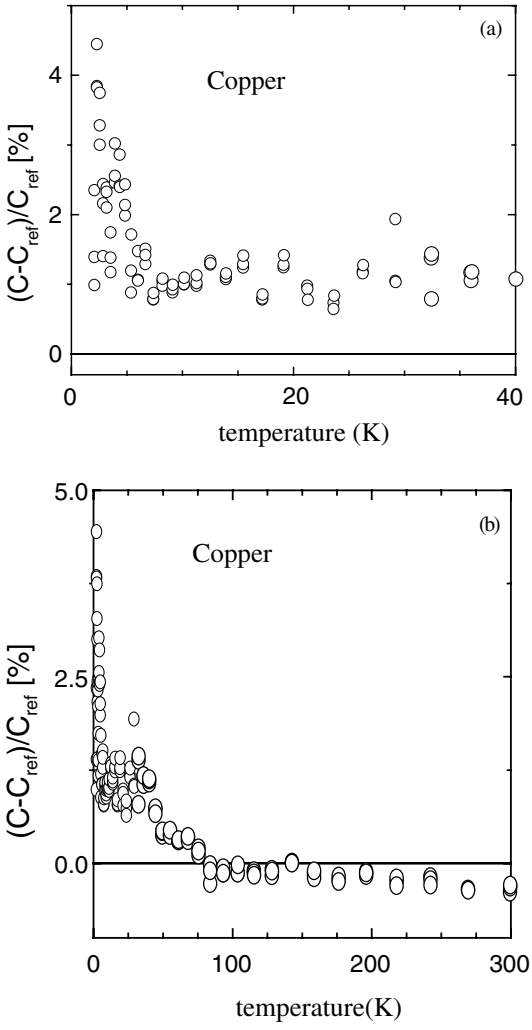

Fig. 2. A plot of the relative deviations from reference copper specific-heat data to that for the PPMS calorimeter at low temperatures (a) and to room temperature (b).

Phillips et al. [20] by 2.4% and 12.4%, respectively. Above 30 K (Fig. 2b) our results fall within 0.75% of the scatter obtained from Martin's measurements with an RMS deviation of 0.95%. As discussed above, a substantial fraction of the deviation below 30 K may be a consequence of temperature-scale and addenda errors. There is noticeable scatter in the Cu deviation plots shown in Fig. 2; this scatter is most apparent below 50 K. The scatter occurs because the PPMS calorimeter has a reduction in point-to-point reproducibility below 50 K. The PPMS reproducibility was experimentally determined by making three measurements at a given temperature and examining the scatter between those data points. Above 50 K the difference between two measurements at a given temperature differ by no more than 0.25%. The point-to-point difference below 20 K can be as large as 1%, with values of 0.5% common. Shown in Fig. 3 is the specific heat of copper measured in the normal manner after slow cooling. After the measurements were made in the normal way, the sample was warmed to room temperature, and then rapidly cooled at a rate of 20 K min^{-1} to 20 K. Three specific-heat points were measured on *cooling* from 20 to 10 K. This temperature-cycling process was repeated three times in order to obtain data from 40 to 30 K. Note that the first point measured in each series is circled. There appears to be a small but noticeable effect in the precision of the first data point in each series.

We examined the error in PPMS specific-heat data as a function of sample mass by measuring gold samples of different masses. Such a comparison provides the lower-limiting, low-mass restrictions for measurements based on sample molar volume and density. Two gold samples from the same batch weighing 4.45 and 87.69 mg were measured. The results as obtained on the PPMS are summarized in Table 1 where they are compared to the literature reference data [22]. The data in Table 1 indicate that the specific-heat values have an uncertainty of

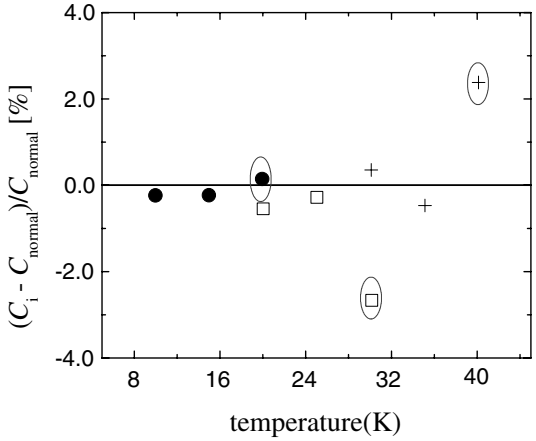

Fig. 3. The specific heat of copper measured after cooling slowly and after rapid cooling from room temperature at 20 K min^{-1}. After the measurements were made in the normal way the sample was cycled to room temperature. Following the rapid cooling from room temperature, three specific-heat points were measured on *cooling* from 20 to 10 K, 30 to 20 K, and 40 to 30 K. The first point measured in each series is circled.

less than 3%, even when the sample is smaller than that of the addenda.

The influence on the accuracy of the measured specific-heat data is illustrated by considering PPMS $C_p(T)$ data obtained on a 7.7 mg synthetic sapphire single crystal. Our results are compared to a reference function obtained from the measurements of [23] as shown in Fig. 4 along with the ratio $C_{\text{sample}}/C_{\text{addenda}}$. Between 100 and 300 K the data lie within 5% of the reference data. Below 100 K, the deviation becomes large, reaching 40% below 10 K. There are reasons for the monotonic rise in the deviation: (1) there is no electron specific-heat contribution to the total specific heat; (2) sapphire has a high Debye temperature and the phonon contribution to the total specific heat is small below 60 K; (3) the low density of sapphire (4 g cm^{-3}) limits the number of

Table 1
Analysis of the specific-heat accuracy as a function of sample mass for high-purity gold

T (K)	$C_{\text{sample}}/C_{\text{addenda}}$	C_{addenda} (μJ/K)	C_{sample} (μJ/K)	Error [%] $(C_{\text{sample}} - C_{\text{ref}})/C_{\text{ref}}$
4.45 mg				
1.932	0.412	0.245	0.101	−0.4
2.380	0.512	0.330	0.169	−0.6
2.649	0.615	0.377	0.232	3.6
3.633	0.688	0.768	0.529	1.5
87.69 mg				
1.890	7.88	0.246	1.94	2.8
2.041	8.22	0.281	2.31	1.9
2.628	9.02	0.490	4.42	2.7
3.208	9.02	0.830	7.49	1.8

C_{sample} is the sample heat capacity measured with the PPMS, C_{ref} corresponds to the expected sample heat capacity at the indicated temperature, $C_{\text{sample}}/C_{\text{addenda}}$ lists the measured ratio of the sample and addenda heat capacities, and the measurement error is determined relative to the C_{ref} data [21].

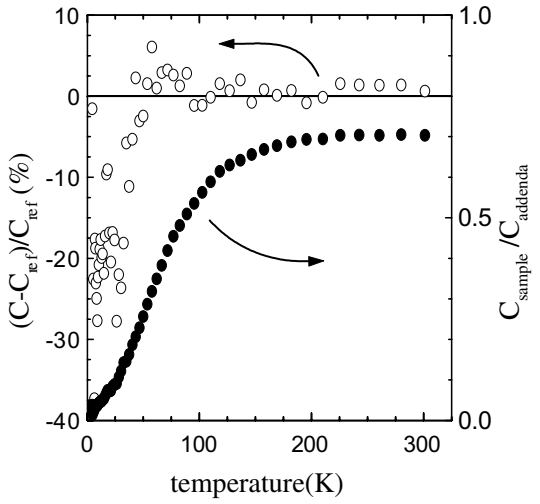

Fig. 4. A plot of the relative deviations of the PPMS sapphire results from the reference specific-heat data [22].

atoms that can be placed on the QD 9 mm^2 sample platform, and the sample-to-addenda heat-capacity ratio drops steadily with decreasing temperature; and, (4) there are large error bars on the reference-data set on the NIST sapphire below 60 K [23], and sample-to-sample variations, including differences in concentrations of O vacancies are common. While $C_{\text{sample}}/C_{\text{addenda}}$ is reasonable (0.7 or greater) above 100 K, the addenda accounts for a majority of the heat capacity below 50 K. The data in Fig. 4 are meant to provide a stringent test of accuracy, and can be typical of what will happen if a PPMS is used with an insulating sample that is too small. In order to insure accurate heat-capacity data, samples for the PPMS should be large enough so that $C_{\text{sample}}/C_{\text{addenda}} > 0.5$ for a metal and greater than 1.5 for an insulator over the temperature region of interest. This is also true for most thermal-relaxation calorimeters. The wide temperature range accessible with the PPMS, coupled with the many orders of magnitude that C_a and C_x can change in going from 1.8 to 400 K, means that considerable attention should be made to sample mass selection. In general, the PPMS calorimeter is designed to measure samples between 10 and 100 mg. While low-T measurements may work well with 10 mg samples, measurements to 300 K and beyond generally require samples closer to 100 mg. In practice a given compound's lower-limiting measurable sample mass is dictated by the compound's electronic specific heat, Debye temperature, and molar volume.

Up to this point we have reported on materials in which there are no phase transitions, and therefore the specific heat does not vary over the thermal-relaxation temperature decay interval ΔT. For a phase transition one might think that this assumption would not hold since the steepness in the specific heat, taken as the change in specific heat evaluated at the maximum jump or transition temperature $\frac{1}{C}\frac{dC}{dT}\big|_{\max}$, can be large for first- and second-order phase transitions. In order to test this assumption we compared the specific-heat data at a first- and second-order transition, both occurring at nearly the same temperature. First, we will consider a second-order transition where there is no latent heat, i.e., the steepness in the specific heat is relatively low; and second, we consider a sharp first-order transition.

4.2. Second-order (continuous) phase transition

For a second-order phase transition we compare the specific heat of the HO transition of the heavy-fermion URu_2Si_2 measured on a PPMS to the measurements of Jaime et al. [24] on a custom-built relaxation calorimeter. The results are shown in Fig. 5. It is evident that similar results are obtained on both calorimeters, and that the total height of the transition is comparable for both measurements. The steepness of the specific heat is a maximum at the transition temperature, $\frac{1}{C}\frac{dC}{dT}\big|_{\max} = 2.0$ K^{-1}, and no latent heat is involved. Therefore, the PPMS fit of the whole thermal-relaxation temperature response in the vicinity of the transition provides satisfactory $C_p(T)$ data. In our experience the best resolution for the PPMS below 25 K is obtained for approximately seven data points per K ($\Delta T = 0.15$ K). The fact that the transition is relatively broad in temperature allows the PPMS to obtain data through the transition that is in favorable agreement with that obtained on another calorimeter.

4.3. Superconducting transition

We tested the ability of the PPMS to measure $Mg^{11}B_2$, a high-temperature superconductor of current

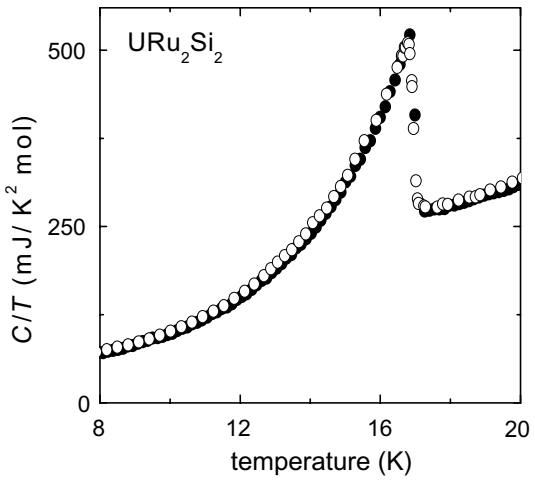

Fig. 5. A comparison of the specific-heat data of the PPMS (●) and a custom-built relaxation calorimeter (○) near the second-order transition in URu_2Si_2.

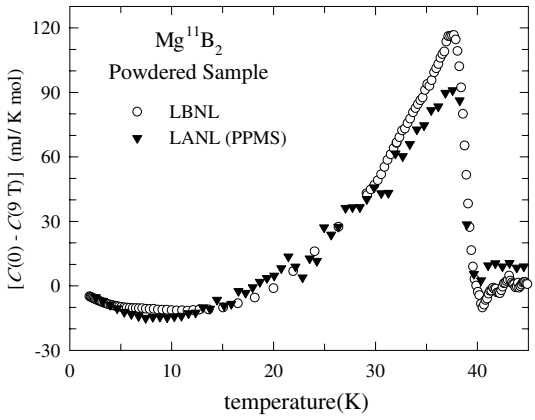

Fig. 6. A comparison of the specific-heat data of the PPMS and a custom-built semi-adiabatic calorimeter at LBNL at the critical temperature for the superconductor $Mg^{11}B_2$.

interest, that has an unusually strong field-dependent specific heat in the mixed state. Fig. 6 compares the discontinuity in the specific heat taken with the PPMS to measurements made on the same sample using a semi-adiabatic calorimeter at LBNL. At the critical temperature, the specific-heat discontinuity is approximately 10% lower than the LBNL measurements. The width of the transition and the critical temperature agree, but the signature feature of the small, non-BCS energy gap at $T = 8$ K is not as pronounced in the PPMS data. The strong dependence of the electronic specific-heat γ on the magnetic field is shown in Fig. 7. Below 2 T there is favorable agreement between the PPMS data and the LBNL data. From 2 to 9 T, the precision of γ is high, while the accuracy is systematically low compared to the LBNL data. We speculate that this discrepancy might be caused by a combination of measuring a powdered sample and no data below 1.8 K to use in an extrapolation of C/T versus T^2.

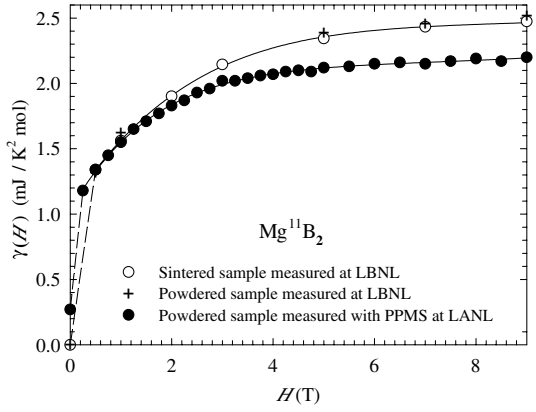

Fig. 7. The electron specific-heat for powdered $Mg^{11}B_2$ as a function of magnetic field measured using the PPMS (●) are compared to those obtained using a custom-built, semi-adiabatic calorimeter at LBNL (○).

4.4. First-order (discontinuous) transition

For the reasons mentioned above, we tested the PPMS on a sharp, first-order antiferromagnetic transition, at approximately the same temperature as the transition in URu_2Si_2, in a single crystal of Sm_2IrIn_8. We have previously measured the same crystal using a custom-built relaxation calorimeter [10] using Bachmann's original measurement approach. The results for both calorimeters are shown in Fig. 8. The data from the custom-built relaxation calorimeter shows a sharp transition near 14.2 K. In contrast, the PPMS data have an anomaly that, while centered at the same temperature, has a shape that appears to be unphysical. When compared to the data obtained from the custom-built calorimeter, we notice two features: Roughly 50% of the transition's height is cut off by the PPMS; and, the PPMS data are low at the base of the transition. As shown in Fig. 9a, an examination of the relaxation data for decays centered near 14.2 K explains the reasons for this peculiar behavior. The system exhibits a first-order transition just below 14.2 K, and, as such, the decay curve is not a simple exponential, but instead has a nearly $dT/dt = 0$ feature in the curve. The erroneous PPMS data stems from the fact that the curve-fitting software cannot properly fit the decay data in Fig. 9a due to the large heat capacity temperature dependence near T_c. At the transition temperature, the steepness in the specific-heat curve reaches a maximum, $\frac{1}{C}\frac{dC}{dT}\big|_{max} = 36.0\ K^{-1}$. We see a change in slope at 14.2 K over a time of approximately 5 s caused by the latent-heat contribution shown in Fig. 9a.

While a time-constant fitting approach cannot adequately determine the specific heat near a first-order transition, the relaxation data can still be used to determine $C_p(T)$ around T_c. This is done by ignoring the automatic PPMS algorithm calculation, and instead applying Eq. (6) to the decay curve when the system

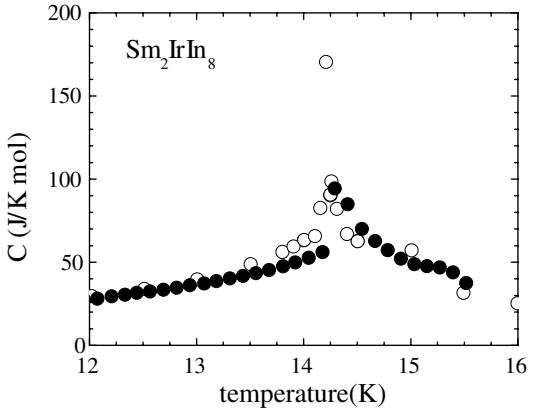

Fig. 8. A comparison of the specific-heat data from the PPMS (●) with that from a custom-built relaxation calorimeter (○) near the first-order transition in Sm_2IrIn_8.

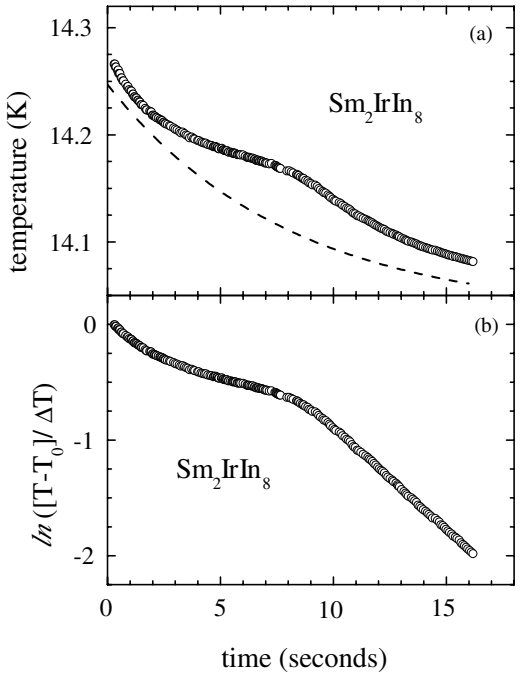

Fig. 9. (a) A plot showing the arrest in the temperature-time relaxation curve at the first-order transition in Sm_2IrIn_8 near 14.18 K (points). The dashed line depicts an exponential-decay curve for comparison (the line is vertically offset for clarity). (b) Plot of thermal-relaxation decay data $\ln[(T - T_0)/\Delta T]$ as a function of time that can be used to determine $C_p(T)$ in the vicinity of a first-order transition.

passes through the transition. The temperature-dependent slope determined from a plot of $\ln[(T - T_0)/\Delta T]$ versus time (Fig. 9b), combined with the thermal conductance K_1 can be used to calculate C_x. The temperature-dependent specific heat determined in this manner is shown in Fig. 10. The data calculated with the conventional PPMS fitting procedure are also shown in the figure. The first-order transition at $T_c = 14.18$ K produces a specific heat of nearly 500 J/mol K at the transition. It is interesting to note that the data obtained via Bachmann's time-constant approach actually agree with the more detailed data, albeit having missed the height of the transition. In contrast, the data obtained with the PPMS curve-fitting approach (solid symbols in Fig. 10) not only miss the transition, but also drastically underestimate the specific heat at the temperatures where points were measured. The additional analysis outlined above can be applied to the PPMS relaxation data using a standard data-analysis program. The addition of this approach to the Quantum Design software would go a long way towards improving the PPMS's ability to determine $C_p(T)$ at a first-order transition.

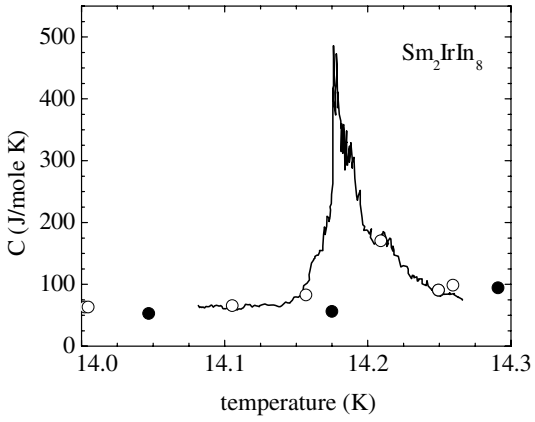

Fig. 10. Properly calculated specific-heat in the vicinity of the first-order transition at $T_c = 14.18$ K in Sm_2IrIn_8 (solid line). For comparison, time-constant fitting data for the custom-built calorimeter (○) and the PPMS curve-fitting data (●) are also presented in the figure.

We have shown that the PPMS does an excellent job on metallic conductors to an uncertainty of ±2% over most of the temperature range $T \approx 5$ to ≈300 K when compared to the best copper measurements, each made on their own temperature scales. Below 5 K the uncertainty increases to ±5% since there are significant deviations in the data, which translate into significant errors in the Debye term. Presumably the scatter, and the error below 5 K, are caused by errors in the temperature scale and the addenda. The results for sapphire illustrate the importance of the sample to addenda ratio when there is no contribution of the electron specific heat at low temperatures.

Results obtained on a second-order phase transition in URu_2Si_2 are in favorable agreement with other data obtained on the same sample using QD's curve-fitting algorithm. At the transition temperature, 14.1 K, the steepness of the specific-heat curve is 2.0 K^{-1}. As a comparison to copper, the steepness of the specific heat evaluated at 14.1 is 0.5 K^{-1}. Results obtained on single crystals of Sm_2IrIn_8indicate that the limitations to measuring sharp, first-order phase transitions arise from a latent-heat contribution that produces a highly nonlinear $\log T$ versus time profile in the relaxation curve. As such, it is not possible to obtain the correct specific heat by fitting the whole temperature response of a heat pulse and the subsequent relaxation. Here the steepness of the specific heat evaluated at the transition temperature is 36.0 K^{-1}. The problem lies not with the calorimetric data, but with the curve-fitting approach used by the PPMS. In its present form, the PPMS system cannot measure the specific heat near a first-order transition; however, an enhancement to the PPMS software would allow the instrument to do so correctly.

Results obtained on $Mg^{11}B_2$ at the critical temperature indicate that the discontinuity is approximately 10% lower than values measured on the same sample at LBNL. For the LBNL measurements several grams of $Mg^{11}B_2$ was required, whereas only 20 mg was used for the PPMS measurements. The dependence of the electron specific heat on magnetic field is pronounced in $Mg^{11}B_2$. Below 2 T, there is favorable agreement between the PPMS and the LBNL measurements. While

the PPMS data above 2 T has good precision, the accuracy falls off to nearly 10%. Although the magnetoresistance of the thermometers are accounted for in the QD magnetic field thermometer calibration routine, we speculate that errors involved with measuring a powdered sample combined with no data below 1.8 K are responsible for the discrepancy.

Acknowledgements

All work was carried out at Los Alamos National Laboratory under the auspices of the United States Department of Energy. Work at the Universtiy of Florida was performed under the auspices of the United States Department of Energy, contract # DE-FG05-86ER45268. We are grateful to D.G. Hinks and J.D. Jorgensen at Argonne National Laboratory for the $Mg^{11}B_2$ samples used in this study. We acknowledge productive discussion with R. Black, R. Dickey, D. Polancic, and R. Fox at QD.

References

[1] Eucken A. Z Phys 1909;10:586.
[2] Nernst W. Sitzb Kgl Preuss Akad Wiss 1910;12:261.
[3] Handler P, Mapother DE, Rayl M. Phys Rev Lett 1967;19:356.
[4] Sullivan PF, Seidel G. Phys Rev 1968;173:679.
[5] Bachmann R, DiSalvo Jr FJ, Geballe TH, Greene RL, Howard RE, King CN, Kirsch HC, Lee KN, Schwall RE, Thomas HU, Zubeck RB. Rev Sci Instrum 1972;43:205.
[6] Schwall RE, Howard RE, Stewart GR. Rev Sci Instrum 1975;46:1054;
Stewart GR, Cort B, Webb GW. Phys Rev B 1981;24:3841;
Stewart GR. Rev Sci Instrum 1983;54:1.
[7] Zink BL, Revaz B, Sappey R, Hellman F. Rev Sci Instrum 2002;73:1841.
[8] Doettinger-Zech SG, Uhl M, Sisson DL, Kapitulnik A. Rev Sci Instrum 2001;72:2398.
[9] Quantum Design, 11578 Sorrento Valley Road, San Diego, CA 92121. http://www.qdusa.com.
[10] Pagliuso PG, Thompson JD, Hundley MF, Sarrao JL, Fisk Z. Phys Rev B 2001;63:4426.
[11] Maple MB, Chen JW, Dalichaouch Y, Kohara T, Rossel C, Torikachvili MS, McElfresh MW, Thompson JD. Phys Rev Lett 1986;56:185.
[12] Bouquet F, Fisher RA, Phillips NE, Hinks DG, Jorgensen JD. Phys Rev Lett 2001;87:47001.
[13] Ema K, Uematsu T, Sugata A, Yao H. Jpn J Appl Phys, Part 1 1993;32(4):1846.
[14] Hwang JS, Lin KJ, Tien C. Rev Sci Instrum 1997;68:94.
[15] Hinks DG, Claus H, Jorgensen JD. Nature 2001;411:457.
[16] Brandt BL, Liu DW, Rubin LG. Lake shore cryotronics. http://www.lakeshore.com; Rev. Sci. Instrum. 1999;70(104).
[17] Wright DA. Relaxation time of Cernox after quench, PhD thesis, Department of Chemistry, University of California-Berkeley, CA 94720, 1996. p. 31.
[18] Holste JC, Cetas TC, Swenson CA. Rev Sci Instrum 1972;43:670.
[19] Martin DL. Phys Rev B 1973;8:5357.
[20] Phillips NE, Fisher RA, Emerson JP, Gordon JE, Woodfield BF, Wright DA, unpublished.
[21] Martin DL. Rev Sci Instrum 1987;58:639.
[22] Boerstoel BM, Zwart JJ, Hansen J. Physica 1971;54:442.
[23] Archer DG. J Phys Chem Ref Data 1993;22(6):1440–53.
[24] Jaime M, Kim KH, McCall S, Mydosh JA. Phys Rev Lett 2002;89, 287201/1-4.